

## ABSTRACT

Title of Document:

SPRAY CHARACTERISTICS FROM FIRE  
HOSE NOZZLES.

Brian Edward Salyers, Master of Science, 2010

Directed By:

Dr. André Marshall, Associate Professor,  
Department of Fire Protection Engineering

This research examines the spray characteristics of fire hose streams. Smooth bore fire hose nozzles create jets with shear column breakup due to high Weber numbers. Laboratory settings produced a cylindrical water jet with the same column breakup behavior. The jet was injected into still air with fully developed turbulent flow. The test nozzle was oriented parallel to the floor. A patternator defined the shape and distribution of the spray. Shadowgraphy measurements determined the flow, drop size and velocity. The spray was tested in the middle of the liquid core.

SPRAY CHARACTERISTICS FROM FIRE HOSE STREAM NOZZLES.

By

Brian Edward Salyers

Thesis submitted to the Faculty of the Graduate School of the  
University of Maryland, College Park, in partial fulfillment  
of the requirements for the degree of  
Master of Science  
2010

Advisory Committee:  
Professor André Marshall, Chair  
Professor Peter Sunderland  
Professor James Milke

© Copyright by  
Brian Salyers  
2010

## Acknowledgements

This research could be conducted thanks to funding from the National Science Foundation. I would like to thank Dr. André Marshall for providing me with this research opportunity. His guidance throughout the last four semesters has been invaluable. Dr. Marshall was extremely helpful by explaining difficult concepts or figuring out better approaches for our research.

Over the last five years the entire faculty and staff of the fire protection engineering department have gone above and beyond in every aspect. They have provided a great education and while giving me a chance to get involved outside of the classroom. I would like to thank my committee, Dr. James Milke and Dr. Peter Sunderland. Both of which I knew freshman year before I was in fire protection and are a major reason I am here now. Both have always kept their doors open to me for questions or advice.

My research team has been a great help. Yinghui was always helpful and without her I would not have been able to complete my research. She worked with me side by side on everything. I would also like to thank Ning who would often lend a hand and offer advice.

Most of all I would like to acknowledge my parents. They have always encouraged and supported me.

# Table of Contents

|   |     |
|---|-----|
| Acknowledgements.....                                 | ii  |
| Table of Contents.....                                | iii |
| List of Tables.....                                   | iv  |
| List of Figures.....                                  | v   |
| Nomenclature.....                                     | vii |
| 1. Introduction.....                                  | 1   |
| 1.1 Motivation.....                                   | 1   |
| 1.2 Research Background.....                          | 2   |
| 1.2.1. Hose Stream Industry.....                      | 2   |
| 1.2.2. Hose Stream Research.....                      | 5   |
| 1.2.3. Atomization of Liquid Jets in Still Gases..... | 7   |
| 1.3. Research Objectives.....                         | 10  |
| 2. Experimental Setup and Procedure.....              | 11  |
| 2. Experimental Setup and Procedure.....              | 11  |
| 2.1 Nozzle Setup and Test Conditions.....             | 11  |
| 2.2 Diagnostics.....                                  | 13  |
| 2.3 Patternator Test.....                             | 16  |
| 3. Results and Analysis.....                          | 20  |
| 3.1 Spray Dispersion.....                             | 20  |
| 3.2 Flow.....   | 23  |
| 3.3 Characteristic Drop Size.....                     | 26  |
| 3.4 Drop Velocity.....                                | 30  |
| 4. Conclusion.....                                    | 31  |
| Bibliography.....                                     | 33  |

## List of Tables

|                               |    |
|-------------------------------|----|
| Table 1: Test Conditions..... | 13 |
|-------------------------------|----|

## List of Figures

|  |    |
|--|----|
| Figure 1.1. Weber numbers for typical operating range of smooth bore nozzles .....   | 4  |
| Figure 2.1. Axis orientation .....   | 12 |
| Figure 2.2. Mid point of liquid core.....  | 12 |
| Figure 2.3. Shadowgraphy test setup (a) front view (b) side view .....   | 14 |
| Figure 2.4. Grid separation .....  | 16 |
| Figure 2.5. Patternator test setup facing jet.....   | 17 |
| Figure 2.6. Patternator test setup side view .....   | 18 |
| Figure 3.1. Shadowgraphy image of the core region at $x/D$ from 150 - 160 .....  | 20 |
| Figure 3.2. Scatter plot with dimensionless drop size, $d/D$ , with a sample core<br>image.....  | 21 |
| Figure 3.3. Contour plot from patternator results of the measured flow flux fraction<br>from spray tubes.....  | 23 |
| Figure 3.4. Flow fraction from shadowgraphy droplets along the vertical cross-<br>stream direction in increments of $D$ , cumulative flow fraction shown as a curve<br>with the origin in the center of the core ..... | 24 |
| Figure 3.5. Flow fraction of spray from patternator along the vertical cross-stream<br>direction in increments of $1.8D$ , cumulative flow fraction shown as a line with the<br>origin in the center of the core ..... | 25 |
| Figure 3.6. Drop size distribution according to droplet volume fraction with line<br>showing the cumulative volume fraction .....  | 27 |
| Figure 3.7. Low flow region drop size distribution according to droplet volume<br>fraction with line showing the cumulative volume fraction .....  | 28 |

Figure 3.8. Dimensionless drop size against the vertical cross-stream direction,  
 $d_{v50}/D$  shown as a line .....29

Figure 3.9. Dimensionless velocity against the vertical cross-stream direction .....30



## Nomenclature

|  |  |
|--|--|
| A  | Area, m <sup>2</sup>   |
| A <sub>p</sub>                               | Area of tube from patternator according to inner diameter, m <sup>2</sup>                  |
| d  | Drop diameter, mm  |
| d <sub>v50</sub>                             | Characteristic drop diameter, mm   |
| d <sub>32</sub>                              | Characteristic drop diameter, mm   |
| D  | Nozzle diameter, mm  |
| l  | Characteristic length, m   |
| l <sub>D</sub>                               | Nozzle diameter as the characteristic length, m  |
| L  | Nozzle length, m   |
| L <sub>b</sub>                               | Length for onset of primary breakup, m   |
| L <sub>c</sub>                               | Liquid core length, m  |
| N  | Number of images   |
| Q <sub>p</sub>                               | Calculated spray flow rate from patternator, m <sup>3</sup> /s                             |
| Q <sub>pm</sub>                              | Measured spray flow rate, Q <sub>p</sub> <sup>''</sup> /A <sub>p</sub> , m <sup>3</sup> /s |
| Q <sub>p</sub> <sup>''</sup>                 | Flow rate flux from patternator, m/s   |
| (Q <sub>p</sub> <sup>''</sup> ) <sub>n</sub> | Normalized flow rate flux from patternator, m/s  |
| (Q <sub>p</sub> ) <sub>T</sub>               | Total spray flow rate from patternator, m <sup>3</sup> /s                                  |
| Q <sub>s</sub>                               | Droplet flow rate from shadowgraphy, m <sup>3</sup> /s                                     |
| (Q <sub>s</sub> ) <sub>T</sub>               | Total droplet flow rate from shadowgraphy, m <sup>3</sup> /s                               |
| r  | Distance from core, m  |
| r <sub>d</sub>                               | Drop Distance from core, m   |
| u <sub>d</sub>                               | Drop velocity, m/s   |

|           |  |
|-----------|--|
| $u_D$     | Nozzle exit velocity, m/s                                  |
| $u_m$     | Maximum drop velocity, m/s                                 |
| $V$       | Volume, $m^3$  |
| $V_d$     | Drop volume, $m^3$   |
| $VF$      | Volume fraction  |
| $We_d$    | Drop Weber number, $\rho_g u_{dl} / \sigma_l$              |
| $We_l$    | Liquid Weber number, $\rho_l u_{Dl} / \sigma_l$            |
| $x$       | Streamwise length, m                                       |
| $X$       | Total streamwise test length, m                            |
| $y$       | Horizontal cross-stream length, m                          |
| $Y_{dof}$ | Depth of field in the horizontal cross-stream direction, m |
| $z$       | Vertical cross-stream length, m                            |

### **Greek Letters**

|            |                             |
|------------|-----------------------------|
| $\rho_g$   | Gas density, $kg/m^3$       |
| $\rho_l$   | Liquid density, $kg/m^3$    |
| $\sigma_l$ | Liquid surface tension, N/m |

### **Subscripts**

|       |                    |
|-------|--------------------|
| $b$   | Breakup            |
| $c$   | Core               |
| $d$   | Droplet            |
| $dof$ | Depth of field     |
| $D$   | Nozzle diameter, m |
| $l$   | Liquid properties  |

|   |              |
|---|--------------|
| m | Maximum      |
| n | Normalized   |
| p | Patternator  |
| s | Shadowgraphy |
| T | Total        |

# 1. Introduction

## 1.1 Motivation

Hose streams are a widely used tool for fire suppression. Water is an effective, cheap and abundant extinguishing agent. Hose streams work by using large diameter water jets at a high velocity to penetrate the fire. Despite their frequent use, there has been little focus on the spray characterization. Performance evaluations are provided by the manufacturer and include empirical testing that varies for each company. These current performance standards involve the trajectory and force of a hose nozzle at varying flows. Hose stream experiments tend to concentrate on the elevated temperature droplet evaporation or the critical water amount dispersed by hose streams to put out fires. Related research to solid jet hose nozzles, also referred to as smooth bore nozzles, includes liquid jets into still air. Using a solid water jet with a Weber number in the same column breakup regime allows for measurements to be extrapolated to different jet diameters.

Spray behavior research could build a bridge connecting the understanding of the heat evaporation of the droplets to write the complete story of hose streams in a fire. NIST hopes to include hose streams for computer modeling in the near future [1]. Accurate implementation cannot occur until the spray distribution, drop size and velocity are known. An understanding of the spray can lead to improved fire fighting tactics along with more effective hose nozzles. Manufacturers could create hose nozzles with optimal and adjustable spray patterns to fit specific fire scenarios.

## 1.2 Research Background

### 1.2.1. Hose Stream Industry

Fire hoses have been used since the 17<sup>th</sup> century [2]. Water was hand pumped from the fire engine through a sewn leather hose. Modern fire departments use hoses in several different ways. Nozzles from Task Force Tips (TFT) [3,4], Akron Brass Company [5] and Elkhart Brass Manufacturing Company [6] were reviewed. Fire hoses can be connected to fire trucks, fire hydrants, water reservoirs or building standpipes. Hose nozzles may also be connected directly to the top of fire trucks. The type of connection depends on the resources and fire scenario. For example, connections to the top of a fire truck typically use master stream nozzles, meaning a nozzle with a rated flow exceeding 1325 lpm at their rated pressure [7]. However a hand held nozzle allows for maneuverability while providing a flow below 1325 lpm.

Hose stream nozzles can be classified as straight stream or fog. Straight stream nozzles are a family of nozzles that includes smooth bore nozzles as well as those that use multiple orifices creating a circular pattern, similar to a typical household showerhead. For smooth bore nozzles the water passes through a cylindrical nozzle to create a solid jet. The solid stream allows for maximum penetration. The liquid core stays intact for a long distance to penetrate to the fire source. Fog nozzles create a water jet surrounded by mist. Fog nozzles absorb more heat due to smaller droplets but compromise jet trajectory and penetration. Multi-purpose nozzles allow for interchanging between using straight stream or fog settings.

A sample of smooth bore nozzles from Akron [5] and Elkhart [6] was used to quantify the typical geometry and flow. The sample included smooth bore nozzles and multi-use nozzles with a smooth bore option. There is variation in geometry

from one smooth bore nozzle to another. Smooth bore nozzles usually include a 3.81 cm or 6.35 cm inlet to the fire hose connection. The nozzles typically range from 24.8 - 27.9 cm in length. Half of the nozzle exit diameters fell within 1.91 - 2.54 cm, with the entire range including 0.32 - 3.49 cm. This leads to an average contraction of 2.8°. Liquid Weber numbers,  $We_l$ , relate inertial forces to surface tension forces and are important for multiphase flows. Weber numbers were calculated using the exit diameter for the characteristic length and velocity from the rated flow with the equation:

$$We_l = \frac{\rho_l u_D^2 l_D}{\sigma_l} \quad (1.1)$$

Water supply to the nozzle can vary depending on the public water resources and pressure losses before entering the nozzle. Therefore nozzles can be rated to flow at uncommonly low or high flows. The typical operating range was defined based on the total number of nozzles operating at a given Weber number condition and shown in Fig. 1.1. The range is defined at the Weber number corresponding to 12.5% and 87.5% of the total operating conditions of the nozzles. The testing condition and regions denoting breakup regimes in Fig. 1.1 will be discussed later.

Hose stream nozzle standards are given in NFPA 1964: Standard for Spray Nozzles [7]. The rated flow and pressure determined by the manufacturer must be used for the NFPA 1964 performance evaluations. In section 4.2.2. of the NFPA standard, the straight stream jets must contain 90% of their discharge at a distance 3 m from the nozzle in a 30.5 cm diameter circle if the nozzle rated discharge is lower than 1325 lpm or in a 38.1 cm diameter circle if the nozzle rated discharge is greater than 1325 lpm. In section A.4.2.3., NFPA recommends rudimentary inspections for

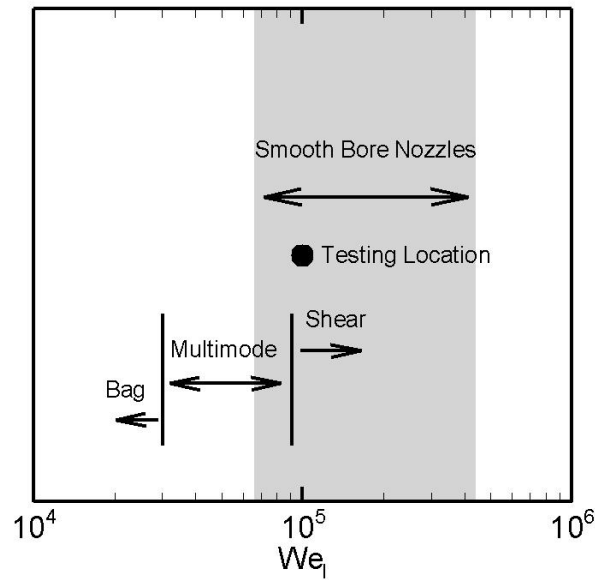


*Figure 1.1. Weber numbers for typical operating range of smooth bore nozzles*

the spray pattern of nozzles. The circumference of the spray should be checked visually for uniformity with no weak areas larger than 2.5 cm at a distance of 61 cm. The thickness of the sheet of the spray 61 cm away should be at least 5.1 cm when the circumference is inspected by hand. Further visual inspection is recommended for no discontinuities in the conical spray shape exceeding 5.1 cm from 61 cm away.

A leading hose nozzle manufacturer, TFT [3,4], details their performance evaluations. The tests are completed inside to neglect wind. The “punch” test measures the force created by the water stream to quantify the penetration capabilities without the effect of elevated temperatures [4]. The nozzles are fixed horizontally. They are tested with a flow of 606 lpm at either 344 or 689 kPa. Circular targets of 7.6, 15.2 or 38.1 cm are placed at a distance of 3.8, 7.6 or 15.2 m from the nozzle. A load cell records the force in pounds allowing impact of different nozzles to be compared with each other.

Another TFT test is for the stream trajectory [3]. The hose is fastened to the floor and then angled 30 ° upward. The stream location is measured using a laser-operated transit. Trajectory plots are provided by TFT for different flows of each hose nozzle. To account for varying discharge angles, TFT provides a supplemental plot to alter the trajectory both horizontally and vertically with the use of height and reach factors.

TFT published a report on different attack procedures [8]. The purpose of the report is to describe the attack approach to maximize the amount of water used. TFT calculates the amount of water needed to absorb enough heat for extinguishment, assuming that 90% of the water is used effectively for heat removal. This calculation assumes that the fire is extinguished by absorbing all of the heat in the volume. Different approaches for hose streams include direct attack for smaller fires, applying the hose stream to the ceiling for blocked fires, or wetting necessary areas to walk through escape. TFT recommends that the stream be applied in a clockwise direction to drive hot gases away from the nozzle based on trial and error. TFT explains that a stationary stream is ineffective because it allows a convection current from the fire to set up around the spray.

### 1.2.2. Hose Stream Research

Rasbash [9] measured the amount of water needed to extinguish fires with furnished volumes from 0.13 – 56.6 m<sup>3</sup>. Smaller tests were completed in model rooms at temperatures of 700 – 900 °C. Extinguishment for smaller tests came from two 0.79 cm water jets from 34.5 – 827 kPa. Small-scale tests show only 3.78 liters were needed per 28.3 m<sup>3</sup>. A fire brigade carried out full-scale tests at 151 lpm and 690 kPa. Full-scale tests range from 30.3 – 37.9 liters per 28.3 m<sup>3</sup> to extinguish a



fire. The critical amount of water was determined when little excess water was left on the floor after testing. Rasbash later reviewed 5 full-scale extinction tests from other hose stream researchers [10]. For each test a critical water rate was found defined as the minimum rate needed to extinguish a post-flashover fire. The critical water rates ranged from 5.6 – 7.4 g/m<sup>2</sup>s. Rasbash analyzed tests carried out in the US and UK that measures the actual amount of water used by fire fighters for fire from 5-60000 m<sup>2</sup> in floor area. Rasbash concluded that the amount of water used in actual fire fighting is about 10-20 times greater than what is needed. A reason given for the discrepancy is the flow rate in real world applications is ten times that of the experiments and leads to an excess of water. More time is needed to extinguish a fire if the critical water rate is used and for fire fighting purposes time is of great importance.

Milke [11] conducted full-scale experiments to simulate hose streams in fires. For 5 tests, water jets were injected into a 22 m<sup>3</sup> room after the fire reached flashover. The nozzle dimensions are not provided but the nozzles were designed to produce a swirling liquid jet with a spray cone of 60°. Droplet measurements were taken 1.52 m from the nozzle along the stream at the lateral edge of the spray cone with a strobe and camera setup. Volume median droplet sizes ranged from 0.48 – 0.63 mm.

Grant [12] provided a comprehensive review of water sprays for fire suppression. Grant discussed in detail the droplet evaporation and heat transfer for elevated temperatures. Droplet penetration into a fire is evaluated to determine the reduction of drop size and velocity. When the droplet reaches a surface different interactions of wetting the area are observed depending on the drop size, temperature and velocity.

Grant [12] provided a qualitative discussion regarding fire hose streams spray behavior. The approach of fire hoses is to remove heat from the fuel along with wetting the surrounding area. The primary goal is usually to have the water reach the base of the fire. Water vapor filling the area is a secondary benefit that is not relied on for extinction. Grant addressed the basics of hose stream spray characteristics. The solid jet flow evolves from a cylindrical column to droplets because of internal turbulence and velocity difference with the still air. The subsequent droplets form a polydispersed spray. This suppression goal is in contrast to the manufacturer TFT [8]. The critical water amount estimated by TFT is an aggressive approach of heat removal. TFT assumes the fire's heat is removed by water while Grant's approach of wetting the fire area leads to excess water. Grant supported Rasbash's [10] claim that real world fire fighting applications use a significant amount of excess water. Rasbash stated 10 – 20 times the critical water amount is used while Grant believed the number to be 10 – 100.

### 1.2.3. Atomization of Liquid Jets in Still Gases

Studies have provided background for different column breakup regimes according to Weber number ranges. Birouk and Lekic [13] and Dumouchel [14] classify the atomization regime of liquid jets in ambient air as any liquid jet with  $We_j > 33200$ . The jets are at a high velocity and begin to disintegrate along the liquid core. The disintegration is a stripping behavior where droplets were significantly smaller than the nozzle diameter.

A similar Weber number is found again by Sallam [15] to describe jet column breakup regimes. Scenarios included round water jets injected downward with fully

developed turbulent flow. Weber numbers ranged from 235 – 270000. The experiments involved shadowgraphy from double-pulsed YAG lasers, a procedure discussed further in Section 2.2. When Weber numbers exceeded 30000 the jets were shown to be in bag/shear, also referred to as multimode, breakup mode. At this point the liquid core was distorted by the turbulence causing the parts of the column to be in gaseous crossflow due to the velocity difference with the still air. The distortion produces bag-like structures to break off of the liquid core. As the Weber number increases the droplets are produced from shearing off of the liquid column. No specific Weber number is found from Sallam for the transition. The behavior was similar to nonturbulent jets in gaseous crossflow. Weber number ranges for nonturbulent jets in crossflow have the multimode breakup regime to take place from Weber numbers of 24900 – 91400 and shear breakup regime occurring when Weber numbers are greater than 91400 [16]. From Fig. 1.1 it is seen that typical smooth bore hose nozzles are expected to be in the shear breakup regime.

Sallam [15] expands on a previous correlation for the liquid core based on the Weber number. The liquid core of the jet is considered intact until the core is of comparable size to the drops formed. Wu and Faeth [17] developed the correlation to determine the length of the liquid core in the streamwise direction:

$$\frac{L_c}{D} = 7.40We_t^{0.34} \quad (1.2)$$

This correlation was extended by Sallam to incorporate more cases and provide  $L_c/D$  equations for different Weber number ranges [15]. When Weber numbers exceed 30000 the liquid core correlation becomes independent of Weber number. The

increased flow is balanced out by increased disintegration. The modified correlation becomes:

$$\frac{L_c}{D} = 11.0 \left( \frac{\rho_l}{\rho_g} \right)^{1/2} \quad (1.3)$$

Droplet ranges for typical fire fighting applications as reviewed by Grant [12] are typically between 0.1 mm (fixed nozzles) to 1 mm (sprinklers). However, for hose streams the range is usually from 0.5 mm to 1.5 mm. Yoon [18] conducted extensive research on droplet and velocity distributions for fire suppression purposes. Jets in the shear breakup regime are injected horizontally through a conical nozzle creating a widely dispersed mist spray. Yoon used a Phase Doppler Particle Analyzer to obtain measurements based on laser-induced light scattering.

Wu and Faeth [17] created a correlation for the onset of primary drop breakup along the liquid core based on the Weber number and nozzle diameter. The onset of primary breakup is determined by the location where droplets are first seen.

$$\frac{L_b}{D} = 2000 We_l^{-0.67} \quad (1.4)$$

Experimental measurements ranged from  $We_l$  of 100 – 1100000. As the Weber number increases, the onset location for primary breakup gets closer to the nozzle.

Sallam [19] studied the drop size of high Weber number jets with respect to the streamwise direction,  $x$ . The drop sizes from Sallam are determined by the size of the tip from ligaments completing Rayleigh breakup protruding from the core. The Sauter Mean Diameter,  $d_{32}$ , is a characteristic drop size where the diameter has the same volume to surface area ratio.

$$\frac{d_{32}}{D} = 0.27 \left( \frac{x}{DWe_l^{1/2}} \right)^{1/2} \quad (1.5)$$

The correlation shows that the drop size increases along the streamwise direction because of larger jet disruptions. The drop size decreases as the Weber number increases.

### 1.3. Research Objectives

The research is conducted to develop a process for how to test and analyze the spray characteristics of hose streams. The experiments involve a water jet in the shear breakup regime. The results can be applied to smooth bore hose nozzles of varying diameters. The goal is to quantify the dispersion, flow, drop size and velocity at the midpoint between the nozzle and the end of the liquid core.

## 2. Experimental Setup and Procedure

### 2.1 Nozzle Setup and Test Conditions

The piping is connected to a rigid member perpendicular to the ceiling. The connection allows for the nozzle setup to be moved in the vertical direction. The nozzle is mounted on a plate that has an option of pivoting to test for the flow at different angles. Water is delivered through a smooth cylindrical acrylic tube. The acrylic tube, referred to as the nozzle, has an inner diameter of 1.27 cm. Fully developed turbulent flow is found in fire hoses due to the high velocities and long lengths. To reach fully developed turbulent flow, testing conditions require the L/D to be at least 36 based on a correlation with the Reynolds number [20]. Similar testing uses  $L/D > 40$  as a standard for fully developed turbulent flow [15,17,19]. The nozzle used is 61 cm long and has an L/D of 48. The pressure is recorded before entering the nozzle with a Pitot tube connected to an electronic pressure transducer. Pressure loss calculations from the connection to the piping and through the nozzle are used to determine the nozzle exit stagnation pressure of 300 kPa [20]. The average jet exit velocity, consistent with the flow rate and the pressure reading, is 24 m/s.

Testing was conducted under ambient conditions. The densities of water and air were  $998 \text{ kg/m}^3$  and  $1.2 \text{ kg/m}^3$ . The viscosities of water and air were  $1.003 \times 10^{-3} \text{ kg/ms}$  and  $1.8 \times 10^{-5} \text{ kg/ms}$ . Surface tension of water was taken to be  $0.0728 \text{ N/m}$ .

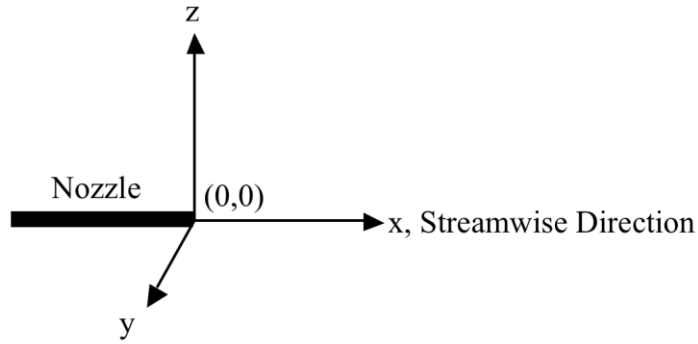


Figure 2.1. Axis orientation

The water jet is injected into still air at a 180 lpm. The flow contains no cavitation. The Weber number of 100000 places the jet in the shear breakup regime, as shown in Fig. 1.1. This Weber number would be comparable to a fire fighting hose nozzle with an inner diameter of 2.9 cm and a flow of 170 lpm. Fig. 2.1 displays the axis orientation for the test setup. The three axes are defined as the streamwise direction  $x$ , the vertical cross-stream direction  $z$ , and the horizontal cross-stream direction  $y$ . The center of the nozzle exit is set as the origin for all measurement.

From Eq. (1.2) the liquid core is estimated to end at  $L_c/D = 317$ , or 4.0 m. Tests are conducted to include the mid point between the nozzle exit and the theoretical end of the liquid core as seen in Fig. 2.2.



Figure 2.2. Mid point of liquid core

For the patternator test, the water is collected at  $x/D$  of 158, or 2.0 m. The shadowgraphy measurements are taken along a 12 cm section in the streamwise direction. Therefore the testing area includes  $x/D$  from 150 to 160. The test conditions are displayed in Table 1.

Table 1: Test Conditions

| Diameter (cm) | Flow (lpm) | $We_1$ | Pressure (kPa) | $x/D$     |
|---------------|------------|--------|----------------|-----------|
| 1.27          | 180        | 100000 | 300            | 150 - 160 |

## 2.2 Diagnostics

Drop size and velocity are measured using shadowgraphy techniques with a LaVision system. The apparatus is placed along the streamwise direction to capture images between 190 - 202 cm as seen in Fig. 2.3. The spray goes through an opening section in the middle of the test setup. Water barriers protect the laser, camera and computer system. A double-pulsed YAG laser is connected with fiber optics to a diffuser. The light output from the diffuser is expanded with a 20 cm Fresnel lens placed 15 cm away from the core of the spray along the horizontal cross-stream direction shown in Fig. 2.3 (a). An Image ProX M4 CCD camera with a 60 mm lens faces the diffuser at a distance of 70 cm from the jet along the horizontal cross-stream direction. Laser pulses are emitted in pairs separated by 80  $\mu$ s. The camera is synchronized to capture particles in the image plane for each laser pulse. A quick laser pulse of 3 - 5 ns allows the images to hold particles as if they are frozen. The diffused light against the Fresnel lens serves as a backlight. The camera records the change in illumination from the water in front of the lit background. An edge detection algorithm in the LaVision SizingMaster program distinguishes droplets and



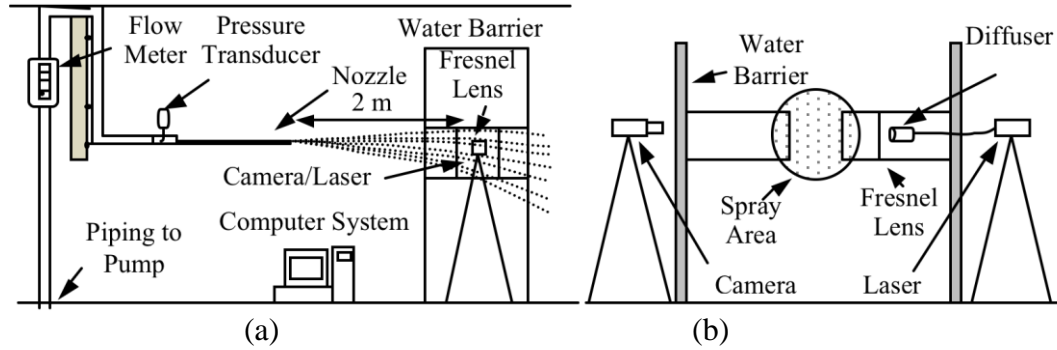


Figure 2.3. Shadowgraphy test setup (a) front view (b) side view

their size with the light intensity difference. A Particle Tracking Velocimetry algorithm then tracks similar particles in the paired images inside of an interrogation window set by the user. Non-spherical particles are not included. The velocity of each droplet is calculated based on the distance divided by the time ( $80 \mu\text{s}$ ) between the paired images. The depth of field for the image area is measured to be 2.8 cm.

Measurements begin after steady flow is established. Measurements are taken in 3 locations along the vertical cross-stream direction to include the majority of the vertical spray width. 200 image pairs are taken for each of the 3 locations. The results are overlapped and combined to show the spray width without breaks between testing locations. Droplets from only one location are included in overlapping areas to prevent over counting. The total amount of droplets used in analyses is about 175000.

The flows from the shadowgraphy measurements are calculated in increments of the nozzle diameter along the vertical cross-stream direction. The flows are evaluated for each drop and summed for each  $D$ . The core and non-spherical drops are not included in the droplet flow calculation. The total droplet flow is derived from:

$$(Q_s)_T = \int u dA \quad (2.1)$$

The velocity used is the streamwise velocity for the flow to be given as the streamwise flow. Cylindrical coordinates are used to derive the droplet flow. This assumes the flow is circular in shape and can be rotated about the center.

$$(Q_s)_T = \iint u_d r_d dr d\theta \frac{V_d}{V} \quad (2.2)$$

The equation is revolved about the streamwise axis. The flow is integrated with separate rotations above the core and below the core. The ratio of the volume from the drops to the total tested volume is used to account for the fact that the entire volume is not filled with water. The equation includes  $\pi$  because flow is calculated in the entire vertical cross-stream direction.

$$(Q_s)_T = \frac{\pi}{N Y_{\text{dof}} X} \sum u_d r_d V_d \quad (2.3)$$

The flow is divided by the number of images, N. Weighting the drops with r (the distance from the core) is necessary to account for the change in area tested. When close to the core only a small amount of the spray is included in the depth of field. Further from the core a higher amount of the spray is in the depth of field.

The characteristic drop size,  $d_{v50}$ , is defined by the median diameter according to the volume distribution. The distance to the core and the streamwise velocity weights the volume fraction. The distance from the core, r, is needed as it was for the flow calculations to account for the change in area. Shadowgraphy measurements have a bias towards slower drops since their slow velocity makes it more likely to “freeze” them in the testing area. The bias is corrected by weighting the velocity in the volume fraction equation. The volume fraction is then:

$$VF = \frac{u_d r_d V_d}{\sum u_d r_d V_d} \quad (2.4)$$

### 2.3 Patternator Test

Collecting water with a grid of tubes perpendicular to the jet creates a patternator. Water is collected in solid smooth acrylic tubes with inner diameters of 0.95 cm. They are spaced 4.6 cm apart in a wire mesh as seen in Fig. 2.4. The simplified grid displayed in Fig. 2.5 limits points to measure one side of the spray in the horizontal cross-stream direction. Symmetry in the horizontal cross-stream direction allows for the entire spray to be accounted for. One column extends past the core to verify for the flow being centered. The grid has the ability to be used for different conditions and therefore water is only collected from the tubes with measureable flow.

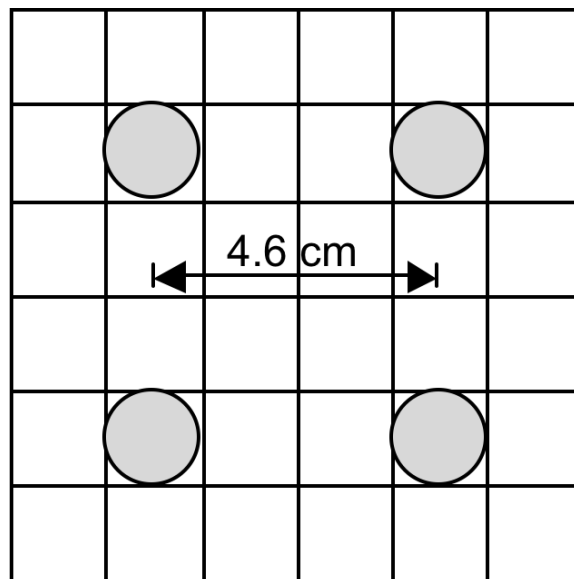


*Figure 2.4. Grid separation*

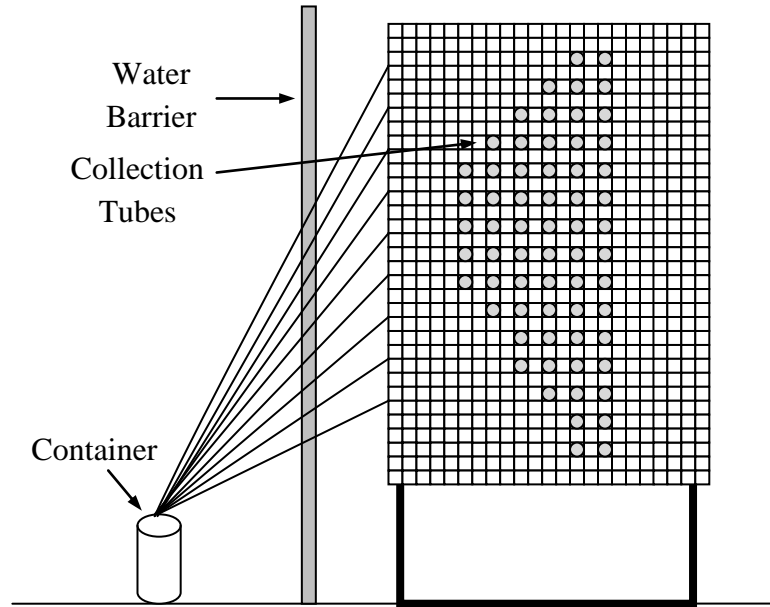


*Figure 2.5. Patternator test setup facing jet*

The side view of the patternator test setup is shown in Fig. 2.6. The acrylic tubes extend 3 cm out from the grid to reduce the effect of water splashing back into the spray and entering the tubes. The tubes are 35 cm in length and connected to a second wire mesh on the other side. The length helps to reduce the splashing effect by distancing the water collection from obstructions. They are angled  $1^\circ$  downward along the streamwise direction for water to continue to flow without a significant effect on the water collection. Larger soft tubing is connected to the back of each acrylic tube. The soft tubing is angled downward through a water barrier where it is collected in a container.

During testing, the water flows until a steady state is reached inside the tubing. Each tube is measured individually. A portion of the outside of the soft tubing is

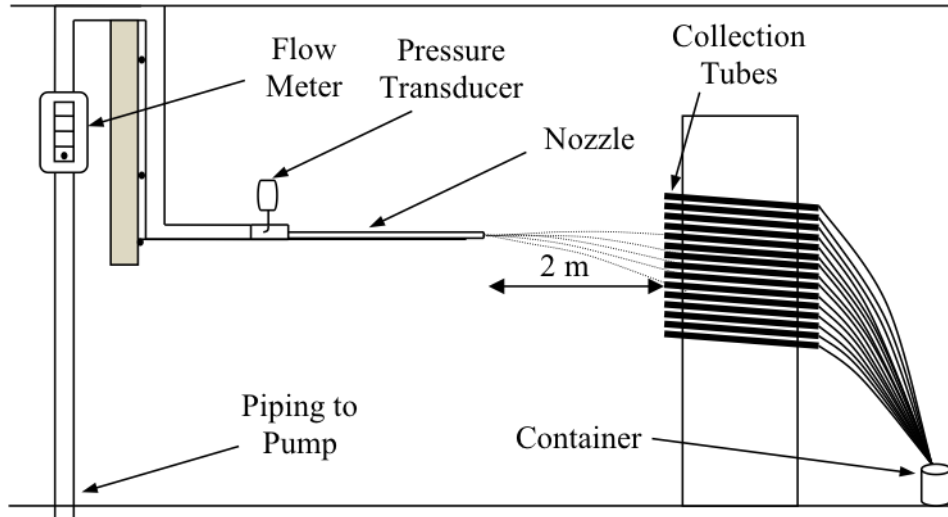


Figure 2.6. Patternator test setup side view

surrounded by cloth to prevent water from running on the outside of the tubing to be collected. The water flows from one tube into a container while the time is recorded. For each point the water volume with time is measured with a beaker and a stopwatch. The measurements are fluxes due to the collection area of the tubes. The grid is shifted horizontally 2.3 cm and the nozzle is raised vertically 2.3 cm to allow for more data points.

The flow flux,  $Q_p''$ , is the recorded flux from each tube. The flow flux is normalized by:

$$(Q_p'')_n = \frac{\sum Q_{pm}}{\sum A_p} \quad (2.5)$$

In Eq. (2.5)  $Q_{pm}$  is the flow measured in each tube. This creates a fraction where the average  $Q_p''/(Q_p'')_n$  will be 1. This flow is the spray flow and does not include the core. This is similar to the shadowgraphy results that only include spherical droplets,

therefore not using the core flow. The length of the core is estimated from shadowgraphy images. The patternator measurements include half of the spray with respect to the horizontal cross-stream direction and are mirrored to create a full picture.

The measurement increments are coarser than shadowgraphy since the patternator tubes are spaced every 1.8D. The flow along the centerline is rotated cylindrically producing the equation for flow for each location:

$$Q_p = Q_p'' \pi r \Delta r \quad (2.6)$$

The distance between tubes is used as  $\Delta r$ . The total flow,  $(Q_p)_T$ , is the summation of the calculated flows from the tubes not including the core.

### 3. Results and Analysis

#### 3.1 Spray Dispersion

The view of the core region from one of the shadowgraphy images at  $x/D$  from 150 - 160 is shown in Fig. 3.1. Gravity bends the core trajectory as seen previously in Fig. 2.2. The test area does not extend long enough in the streamwise direction for the flow to have a measurable decline in trajectory. From the nozzle exit the center of the core is  $6.69D$  (8.5 cm) lower when it enters the testing area. Fig. 3.1 shows that the area around the core in the testing location has a wide distribution of droplet shapes and sizes. At this point bags, ligaments, and drops break off of the core and a smooth cylindrical jet is rarely seen in the images.

The jet trajectory is unaffected by gravity the closer it is to the nozzle. Disintegration begins with shearing of small drops at the onset of primary breakup. From Eq. (1.4) the onset of breakup occurs very early at  $0.89D$ .

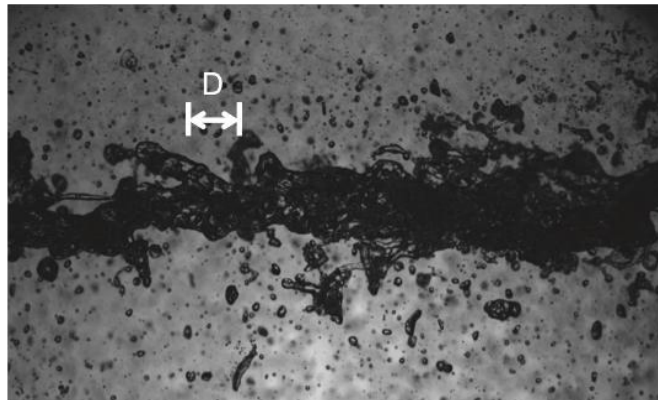


*Figure 3.1. Shadowgraphy image of the core region at  $x/D$  from 150 - 160*

The breakup occurs close to the nozzle because it has a high Weber number. The column breakup immediately following the nozzle exit involves solely small droplets shearing off of the jet. The core trajectory and diameter decline along the streamwise direction. The amount of core disruption is shown to increase as seen in Fig. 3.1 when compared to the jet at the nozzle exit. Primary breakup in the testing location causes large amounts of the core to be stripped off creating ligaments or drops. The jet diameter for the testing area is estimated to have decreased 15% from the original diameter based on measurements in images where the core remained cylindrical. The flow in the core has decreased to 72% of the initial nozzle exit flow. Most of the flow

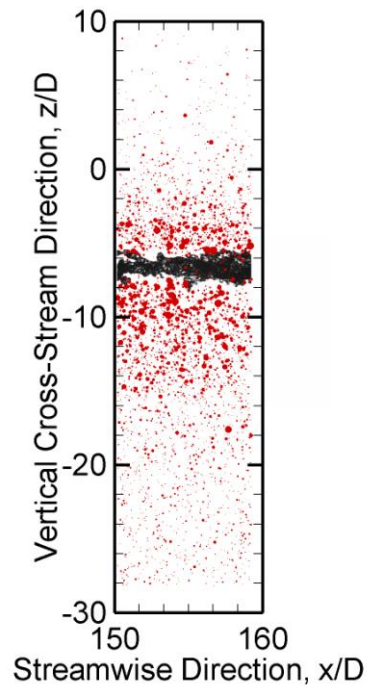


*Figure 3.2. Scatter plot with dimensionless drop size,  $d/D$ , with a sample core image*



has been kept in the core when it arrives at the testing location. The testing location is placed so that it is at the mid point of the liquid core length. A decrease in diameter of 15% at the mid-point of the liquid core length shows that the core diameter does not decrease with linearly. The diameter decline begins minimal at the nozzle and increases along the streamwise direction.

Fig. 3.2 displays the dimensionless droplet sizes in the entire recorded spray width with a sample image imposed on the data. The vertical spray width is defined as the measurable droplet area in the vertical cross-stream direction. The core area does have a small amount of drops due to fluctuations. The spray width extends slightly below the tested area, but later calculations show the flow has significantly decreased by this point.

A clear difference can be seen between the spray near the core and the spray with smaller drops of the outer area. Many droplets around the core will produce secondary breakup into smaller drops due to their large size and velocity. A drop with a drop Weber number above 12 causes droplet bag breakup where the droplet ruptures and produces many smaller drops [21]. Secondary breakup occurs for 3910 drops, or 2.2%. The area outside of the core includes small droplets that are the result of secondary breakup or droplets that sheared off the jet closer to the nozzle.

The main purpose of the patternator is to define the shape of the spray. Fig. 3.3 uses the patternator test results to create a contour plot comparing the spray flow flux fraction,  $Q''_p/(Q''_p)_n$ . The core length is estimated to be about 5D from Fig. 3.1 and not included for the spray flow from the patternator. The core length is large because of deformations. Generally a circular shape is seen. The circular shape is stronger

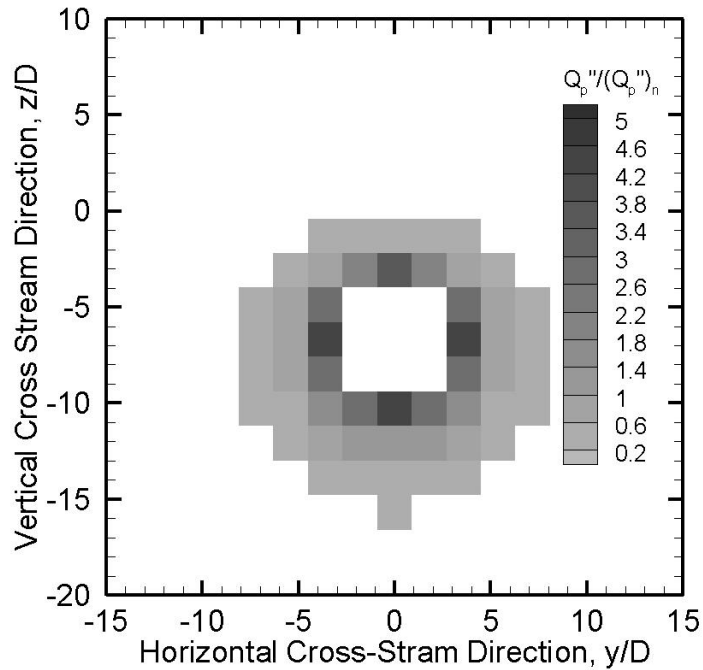


*Figure 3.3. Contour plot from patternator results of the measured flow flux fraction from spray tubes*

closest to the core and becomes more elliptical farther from the core. The bottom portion of the spray extends slightly further because of the effect of gravity. The spray is wider below the core because gravity helps initiate the breakup. The spray directly surrounding the core has significantly greater flow than the remaining area. The spray area appears smaller with the patternator than from the shadowgraphy results. This could be due to limits in water collection through the tubing.

### 3.2 Flow

Fig. 3.4 shows the flow fraction from the droplets along the vertical cross-stream direction from shadowgraphy results. The flow is for droplets only and does not include the core or nonspherical drops. The core is shown 6.69D below the initial

nozzle location. It is seen that the core region contains little drop flow since the fluctuations have a length of approximately  $5D$ , as discussed previously. The droplet flow peaks outside of the core region. Testing restrictions limited the measurements to approach a flow fraction of 0.0006 at the top of the spray and 0.0036 at the bottom. The outlying flow is considered negligible for the calculations.

Distinct differences in droplet size, amount and velocity are seen in the high-flow region surrounding the core. A high flow region is labeled in Fig. 3.4. The region is defined with a cutoff value where different flow behavior is seen. The high flow region includes the middle area of the spray width when  $Q_s/(Q_s)_T$  is above 0.02. The low flow region includes the flow area above and below the high flow area. The high

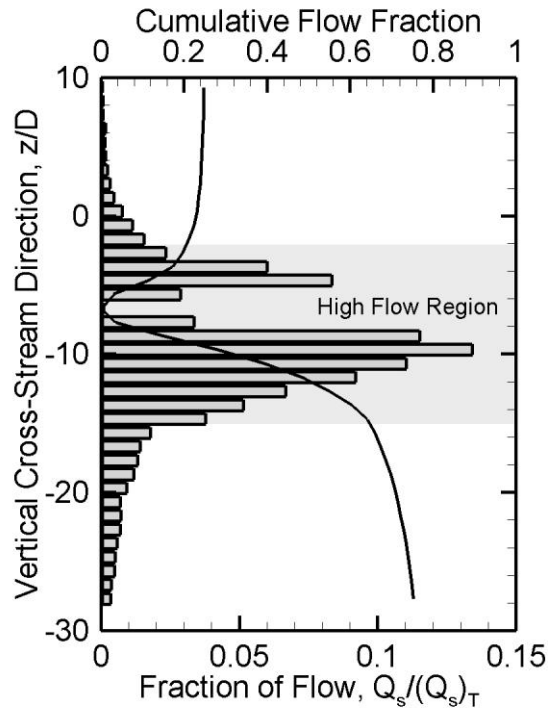


*Figure 3.4. Flow fraction from shadowgraphy droplets along the vertical cross-stream direction in increments of  $D$ , cumulative flow fraction shown as a curve with the origin in the center of the core*

flow region is 13D in length and contains 84% of the droplet flow. For a hose stream the high flow region is important to enable a long trajectory and deep penetration to the fire. The cumulative flow fraction expands out from the center of the core flow. A similar trend of flow fraction and cumulative flow fraction occurs above and below the core but with a different scale. Below the core has greater flow that extends farther out from the core. The bottom flow accounts for 75% of the total droplet flow while the top contains 25%.

The total droplet flow is 9% of the initial flow at the nozzle exit. The core flow is 72% of the initial flow as previously discussed. The ligaments and bags breaking off of the core mostly account for the remaining 19%. The flow from the bags and

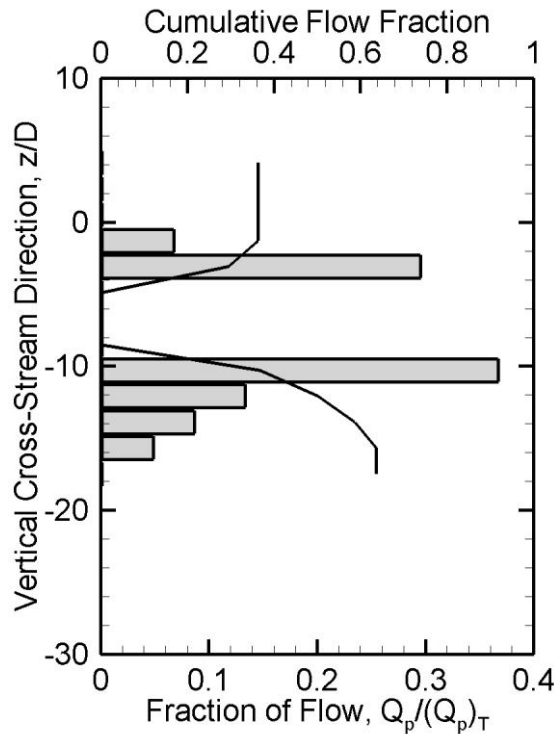


*Figure 3.5. Flow fraction of spray from patternator along the vertical cross-stream direction in increments of 1.8D, cumulative flow fraction shown as a line with the origin in the center of the core*

ligaments are not calculated but from Fig. 3.1 they can be seen to be a significant amount of the flow in the testing area. Minor amounts of flow are also lost in the small drops that shear off around the nozzle after the onset of primary breakup. These droplets would not be seen at  $x/D$  of 150.

Flow measurements from the spray of the patternator test are shown in Fig. 3.5. The measurement region is smaller than in Fig. 3.4. The results take place mostly in the high flow region. The spray flow is distributed 36% above the core and 64% below the core. The core flow is not included in the total flow. When the core flow is compared to the flow from the spray, the spray accounts for 11% of the flow and the core accounts for the remaining 89%. The patternator flow shows slight discrepancies with the shadowgraphy results. This is possibly a result of the coarse grid, water collection method, or the inability to differentiate spherical droplets.

### 3.3 Characteristic Drop Size

The primary suppression goal of hose streams is to penetrate the base of the fire as explained by Grant [12]. Therefore the characteristic drop size important for hose streams is the volume median drop size,  $d_{v50}$ . The histogram for drop size distribution is shown in Fig. 3.6. The  $d_{v50}$  for the spray is 1.7 mm or  $d/D = 0.13$ . A peak is seen at  $d/D$  of 0.1 but a normal distribution is not found. The histogram shows there are more small drops with the distribution stretched to include the larger drops. The drop size distribution above the core is identical to the distribution below the core and can be attributed to the large droplets surrounding the core dominating the volume fraction.

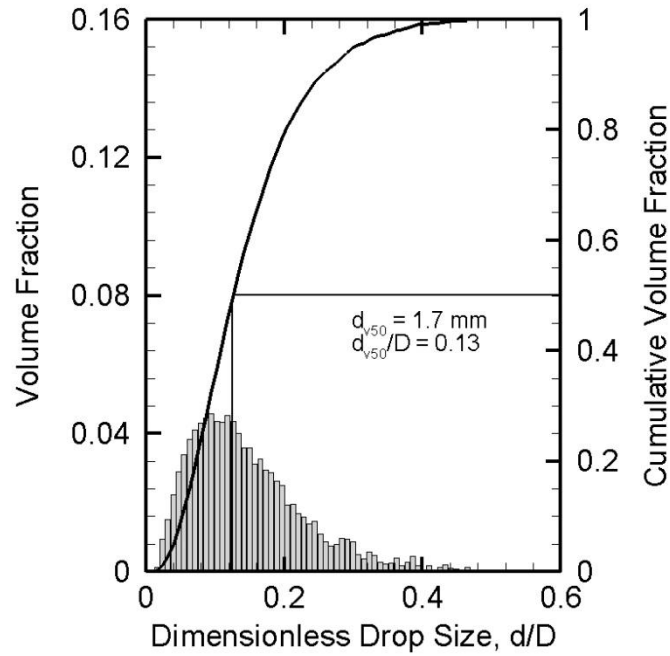


*Figure 3.6. Drop size distribution according to droplet volume fraction with line showing the cumulative volume fraction*

The high-flow range accounts for 89% of the volume fraction and therefore dominates the distribution in Fig. 3.6. The drop size distribution of the low flow region is shown in Fig. 3.7. A different distribution is seen with the peak around  $d/D$  of 0.05. The  $d_{v50}$  for the low flow region is 0.98 mm or  $d/D = 0.077$ . The low flow region shows smaller droplets in a more narrow range.

Surface area is important for fire suppression because of heat extraction, a secondary benefit from hose streams. The equation of  $d_{32}$  is weighted as discussed earlier for  $d_{v50}$  to become:

$$d_{32} = \frac{\sum u_d r_d d^3}{\sum u_d r_d d^3} \quad (3.1)$$

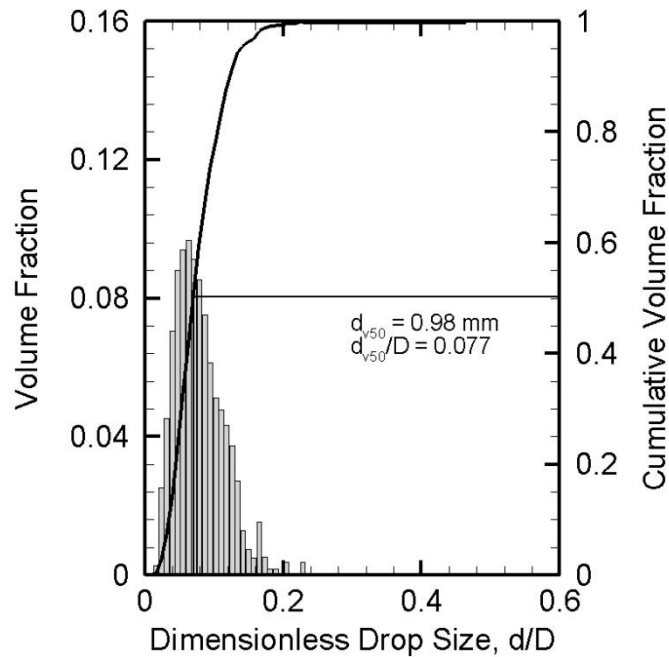


*Figure 3.7. Low flow region drop size distribution according to droplet volume fraction with line showing the cumulative volume fraction*

Over the entire testing region  $d_{32}$  is 1.4 mm or  $d_{32}/D$  of 0.11. The result remains unchanged when considering only the high flow region. The low flow region has characteristic drop sizes of  $d_{32}$  of 0.88 mm or  $d_{32}/D$  of 0.069. The theoretical  $d_{32}$  from Eq. (1.5) estimates the drop size to be 2.4 mm or  $d_{32}/D$  of 0.19. The difference can be accounted for in a different approach for determining the drop size. The theoretical equation is determined by the size of the tip from ligaments completing Rayleigh breakup protruding from the core. The equation only estimates droplets at the core. Sallam's equation does not account for smaller droplets that also appear to surround the core. If only droplets with a Weber number high enough to complete secondary breakup are considered then the  $d_{32}$  is 2.7 mm or  $d_{32}/D$  of 0.21. This number is closer

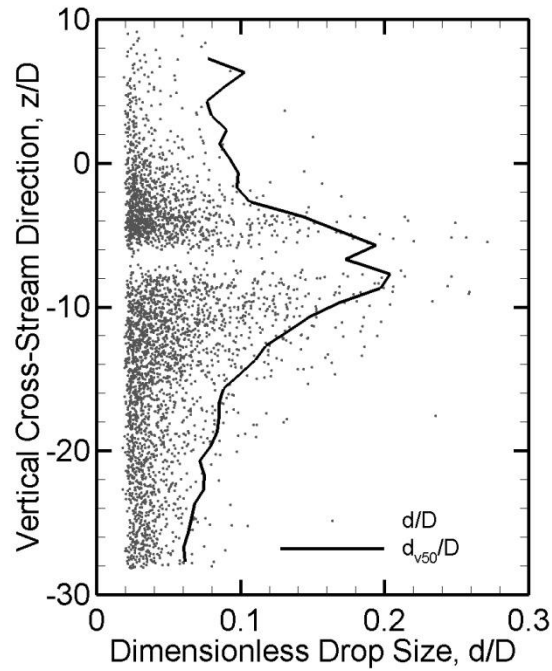


*Figure 3.8. Dimensionless drop size against the vertical cross-stream direction,  $d_{v50}/D$  shown as a line*

to Sallam's estimation because it includes only the large drops moving around the speed of the core.

Fig. 3.8 displays the dimensionless drops sizes along the vertical cross-stream direction. The high flow area has many droplets of a wide distribution of sizes. Some droplets are seen in the core region because of fluctuating behavior discussed earlier. Areas outside of the high flow lack larger drops. This is shown as the  $d_{v50}/D$  increases at the core. As expected, more droplets are below the core compared to above. The drop density above the core becomes thin.



### 3.4 Drop Velocity

Drops closer to the core move faster as shown in Fig. 3.9. The maximum streamwise drop velocity, approximately the core speed, nondimensionalizes the streamwise velocities from the drops. The core speed has shown no measurable decrease in velocity at the testing location. When compared to Fig. 3.8 it is seen that the distance from the jet is a more important factor than the drop size. The drop velocity above the core decreases quicker along the vertical cross-stream direction.

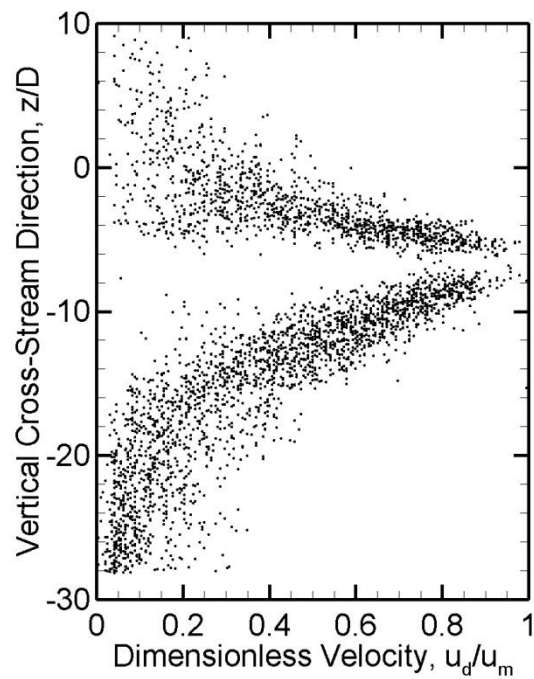


Figure 3.9. Dimensionless velocity against the vertical cross-stream direction

## 4. Conclusion

Experiments quantified the spray characteristics of a round jet in the shear breakup regime oriented parallel to the floor. The spray is examined halfway between the nozzle and the theoretical end of the liquid core. Testing included a patternator and shadowgraphs. The patternator collected water along the streamwise direction with a grid of 0.95 cm tubes. The patternator established the shape of the spray. Shadowgraphy obtained images over the spray width. Drop size, flow, velocity and spray distribution were found from the images. The major conclusions are:

- 1) The droplet spray inside the shadowgraphy testing area contains 9% of the initial nozzle exit flow. Core flow accounts for 72%. Most of the remaining flow is attributed to ligaments or non-spherical drops. The high flow region surrounding the core contains 84% of the droplet flow.
- 2) The  $d_{v50}/D$  and  $d_{32}/D$  of the droplet spray are 0.13 and 0.11. The drop distribution favors smaller drops. The  $d_{v50}/D$  and  $d_{32}/D$  of the low flow region are 0.077 and 0.069.
- 3) The spray behavior below the core contains more drops over a wider range than above the core. The flow from drops was distributed 75% below the core and 25% above the core. The spray from patternator and shadowgraphy is an elliptical shape.

The high flow region is of most importance for hose streams. Smooth bore nozzles rely on the core staying intact to deliver large amounts of water to the fire

through a solid jet. The approach will lead to excess water but the water can be limited when there are less droplets outside of the core region.

The experiments developed a test setup, conditions and process to allow for further exploration of the research. More is needed to fully understand the spray. Testing the entire liquid core will confirm the length and allow the core disintegration to be correlated along the streamwise direction. Different flows and diameters can be used to see how the characteristics scale for other scenarios. Hose streams are typically oriented at an angle. Further tests can determine the effect of the nozzle angle on the spray.

## Bibliography

- [1] Stroup, D., “Hose Stream Characterization and Effectiveness Modeling”, *National Institute of Standards and Technology*, Gaithersburg, MD, 2007.
- [2] Sutton, P., *Jan van der Heyden (1637 – 1712)*, Yale University Press, 2006.
- [3] Task Force Tips, Inc., “Range and Trajectory Data of Hand Held Nozzles”, 1994.
- [4] Task Force Tips, Inc., “The Comparison of Various Types of Nozzles Operating at Specific Flows and Pressures and their Effect on the Impact or Punch of Fire Streams”, 2001.
- [5] Akron Brass Co., “All Nozzles Catalog”, 2009.
- [6] Elkhart Brass Manufacturing Company, “Catalog F”.
- [7] NFPA 1964: Standard for Spray Nozzles, 2008.
- [8] Oster, G., Wiseman, J., “Balanced Fire Attack”, Task Force Tips.
- [9] Nash, P., Rasbash, D., “The Use of Water in Fire-Fighting”, *Fire Research Station*, Boreham, England, 1955.
- [10] Rasbash, D., “The Extinction of Fire with Plain Water: A Review”, *Fire Safety Science-Proceedings of the First International Symposium*, pp. 1145-1163, 1986.
- [11] Milke, J., Evans, D., Hayes Jr., W., “Water Spray Suppression of Fully-Developed Wood Crib Fires in a Compartment”, NBSIR 88 3745, *National Bureau of Standards*, 1988.

- [12] Grant, G., Brenton, J., Drysdale, D., “Fire Suppression by Water Sprays”, *Progress in Energy and Combustion Science*, Vol. 26, pp. 79-130, 2000.
- [13] Birouk, M., Lekic, N., “Liquid Jet Breakup in Quiescent Atmosphere: A Review”, *Atomization and Sprays*, Vol. 19, pp. 501-528, 2009.
- [14] Dumouchel, C., “On the Experimental Investigation on Primary Atomization of Liquid Streams”, *Experiments in Fluids*, Vol. 45, pp. 371-422, 2008.
- [15] Sallam, K., Dai, Z., Faeth, G., “Liquid Breakup at the Surface of Turbulent Round Liquid Jets in Still Gases”, *International Journal of Multiphase Flow*, Vol. 28, pp. 427-449, 2002.
- [16] Ng, C., Sankararisham, R., Sallam, K., “Bag Breakup of Nonturbulent Liquid Jets in Crossflow”, *International Journal of Multiphase Flow*, Vol. 31, pp. 241-259, 2008.
- [17] Wu, P., Faeth, G., “Onset and End of Drop Formation Along the Surface of Turbulent Liquid Jets in Still Gases”, *Physic of Fluids*, Vol. 7, pp. 2915-2917, 1995.
- [18] Yoon, S., Kim, H., Hewson, J., “Effect of Initial Conditions of Modeled PDFs on Droplet Characteristics for Coalescing and Evaporating Turbulent Water Spray Used in Fire Suppression Applications”, *Fire Safety Journal*, Vol. 42, pp. 393-406, 2007.
- [19] Sallam, K., Dai, Z., Faeth, G., “Drop Formation at the Surface of the Plane Turbulent Liquid Jets in Still Gases”, *International Journal of Multiphase Flow*, Vol. 25, pp. 1161-1180, 1999.
- [20] White, F., *Fluid Mechanics*, Sixth Edition, Mc-Graw Hill, 2008.

- [21] Pilch, M., Erdman, C., “Use of Breakup Time Data and Velocity History Data to Predict the Maximum Size of Stable Fragments for Acceleration-Induced Breakup of a Liquid Drop”, *International Journal of Multiphase Flow*, Vol. 13, pp. 741-757, 1987.